LETTER

Operando pH Measurements Decipher H$^+$/Zn^{2+} Intercalation Chemistry in High-Performance Aqueous Zn/δ-V$_2$O$_5$ Batteries

Xu Liu, Holger Euchner, Maider Zarrabeitia, Xinpei Gao, Giuseppe Antonio Elia,* Axel Groß, and Stefano Passerini*

ACCESS | 📊 Metrics & More | 📖 Article Recommendations | 🆂ℹ Supporting Information

ABSTRACT: Vanadium oxides have been recognized to be among the most promising positive electrode materials for aqueous zinc metal batteries (AZMBs). However, their underlying intercalation mechanisms are still vigorously debated. To shed light on the intercalation mechanisms, high-performance δ-V$_2$O$_5$ is investigated as a model compound. Its structural and electrochemical behaviors in the designed cells with three different electrolytes, i.e., 3 m Zn(CF$_3$SO$_3$)$_2$/water, 0.01 M H$_2$SO$_4$/water, and 1 M Zn(CF$_3$SO$_3$)$_2$/acetonitrile, demonstrate that the conventional structural and elemental characterization methods cannot adequately clarify the separate roles of H$^+$ and Zn^{2+} intercalations in the Zn(CF$_3$SO$_3$)$_2$/water electrolyte. Thus, an *operando* pH determination method is developed and used toward Zn/δ-V$_2$O$_5$ AZMBs. This method indicates the intercalation of both H$^+$ and Zn^{2+} into δ-V$_2$O$_5$ and uncovers an unusual H$^+$/Zn^{2+}-exchange intercalation—deintercalation mechanism. Density functional theory calculations further reveal that the H$^+$/Zn^{2+} intercalation chemistry is a consequence of the variation of the electrochemical potential of Zn^{2+} and H$^+$ during the electrochemical intercalation/release.
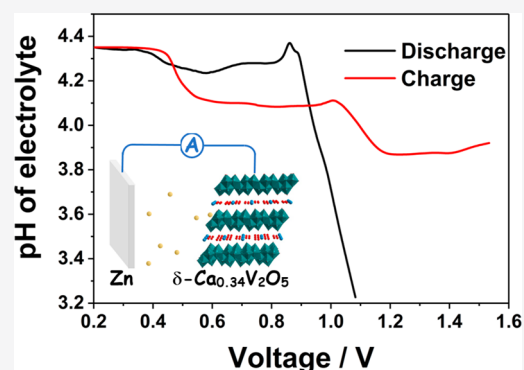
Aqueous zinc metal batteries (AZMBs) are a promising complementary technology to the state-of-the-art lithium-ion batteries for large-scale stationary energy storage because of their sustainability,[1] low cost,[2] safety,[3,4] and high energy density among aqueous batteries.[5−7] Since σ-Zn$_{0.25}$V$_2$O$_5$ was employed as an intercalation-type cathode material for AZMBs in 2016,[8] vanadium oxides have been extensively investigated.[3,9,10] The R&D efforts resulted in the rational design of their structure,[11,12] morphology,[13,14] and addition of secondary components,[15,16] enabling high specific capacities (more than 300 mAh g^{-1} at 50 mA g^{-1}) and prolonged cycle life (hundreds of cycles at 500 mA g^{-1}).[4,17] Nevertheless, the fundamental questions, i.e., which/how species are intercalated into these vanadium oxides, are still under debate.

Although many different characterizations are used in the studies mentioned above, typically, X-ray diffraction (XRD) is the main tool providing the evidence supporting the respective mechanisms. During the operation of many reported vanadium oxides,[7,8,26−29,18−25] two main phenomena, reversible peak shifts of the initial phase and reversible appearances of basic zinc salts (BZSs) at low potentials, are often observed in the XRD patterns. Different explanations are given in the literature

for these phenomena, involving the intercalation of H$^+$,[29] Zn^{2+},[7] and their combination.[21] The peak shifts indicate solid solution processes, going along with a changing interlayer distance. Zn^{2+}, the main cation in the commonly used aqueous electrolytes, is widely considered responsible for the shrinking interlayer distance during the discharge process.[8,18,19,25] However, the possibility of H$^+$ intercalation, which could also contribute to the interlayer shrinking, is neglected. The appearance of BZSs, e.g., Zn$_{12}$(CF$_3$SO$_3$)$_9$(OH)$_{15}$,[30] upon discharge depends on the employed aqueous electrolytes.[24,27,29,31,32] Because the formation of BZC compounds is favored by the increasing electrolyte pH values upon discharge, they have been proven to be an indicator for the reversible H$^+$ intercalation.[27,31] Thereafter, the Zn^{2+} intercalation process was widely doubted by the scientific
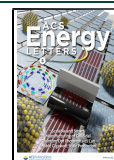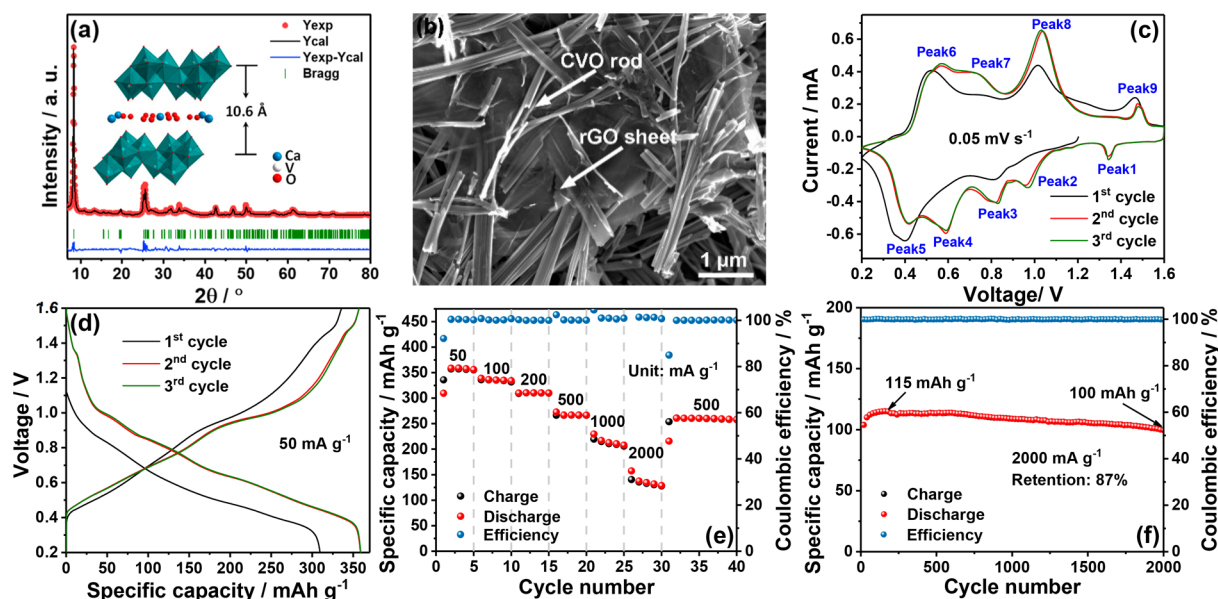
Figure 1. (a) XRD refinement of as-prepared CVO/rGO and the crystal structure model of the CVO. (b) SEM image of as-prepared CVO/rGO. (c−f) Electrochemical performance of the as-fabricated CVO/rGO electrode. (c) CV curves measured at 0.05 mV s^{-1}. (d) Charge−discharge profiles at 50 mA g^{-1}. (e) Specific capacity and Coulombic efficiency obtained at different specific currents. (f) Specific capacity and Coulombic efficiency of cycling at 2000 mA g^{-1}. Coin cell, 3 m Zn(OTF)$_2$ aqueous electrolyte.
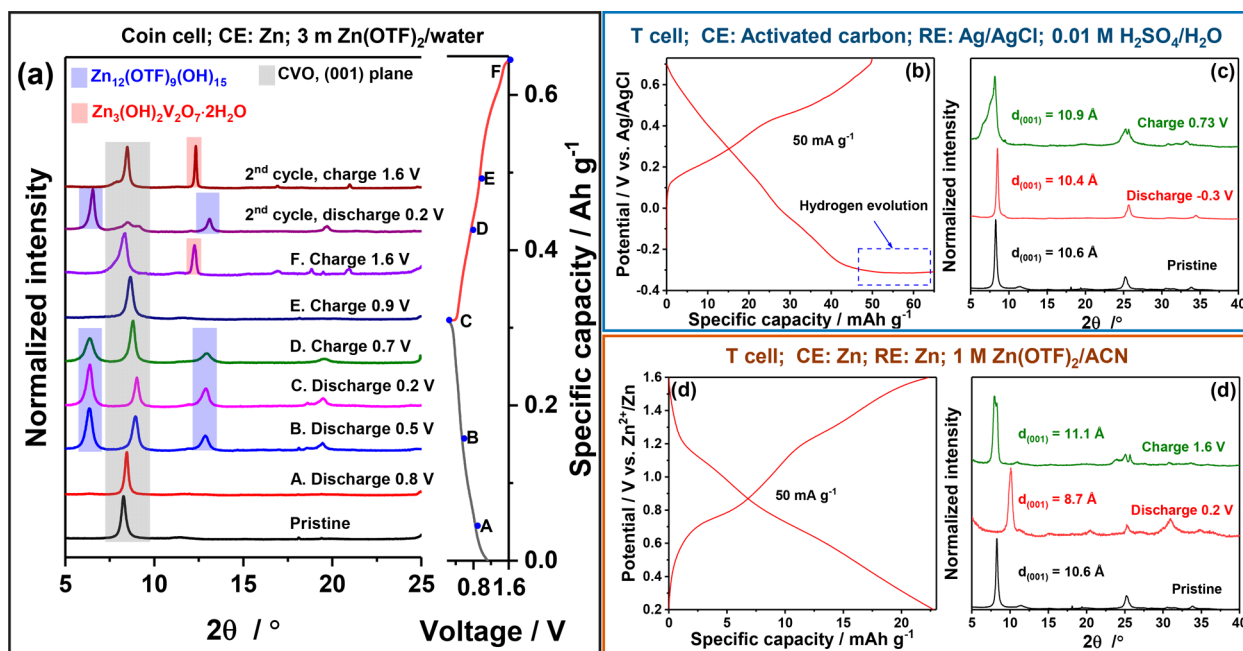

Figure 2. (a) Ex situ XRD patterns of cycled CVO/rGO electrodes at different states of charge during the first and second cycles (coin cell, 3 m Zn(OTF)$_2$ aqueous electrolyte). Charge−discharge profiles and *ex situ* XRD patterns at different states of charge of CVO/rGO electrodes in (b and c) 0.01 M H$_2$SO$_4$/H$_2$O and (d and e) 1 M Zn(OTF)$_2$/ACN electrolytes, respectively. CE is the counter electrode. RE is the reference electrode.

community,[33] as the intercalation of multivalent cations is believed to be difficult and sluggish,[34] whereas vanadium oxides exhibit a decent specific capacity and rate capability in AZMBs. Apparently, the role of H$^+$ and Zn^{2+} intercalations in the vanadium oxides-based AZMBs still needs to be clarified, requiring further experimental evidence. Deciphering the intercalated carriers is not trivial, as it may guide scientists to further optimize cathode materials and electrolytes for better-performing AZMBs.

In this work, high-performance δ-calcium vanadium oxide bronze/reduced graphene oxide (CVO/rGO) was used as a model material to investigate the widely explored but still debated intercalation mechanism.[24,35,36] CVO/rGO was prepared via an efficient microwave reaction (Figure S1) and has been confirmed to be composed of submicrometric δ-Ca$_{0.34}$V$_2$O$_5$·1.16H$_2$O rods on micrometric rGO sheets (1.9 wt %) via XRD, SEM, EDS, Raman spectra, ICP-OES, and TGA (as shown in Figure 1a,b and S2−S4).
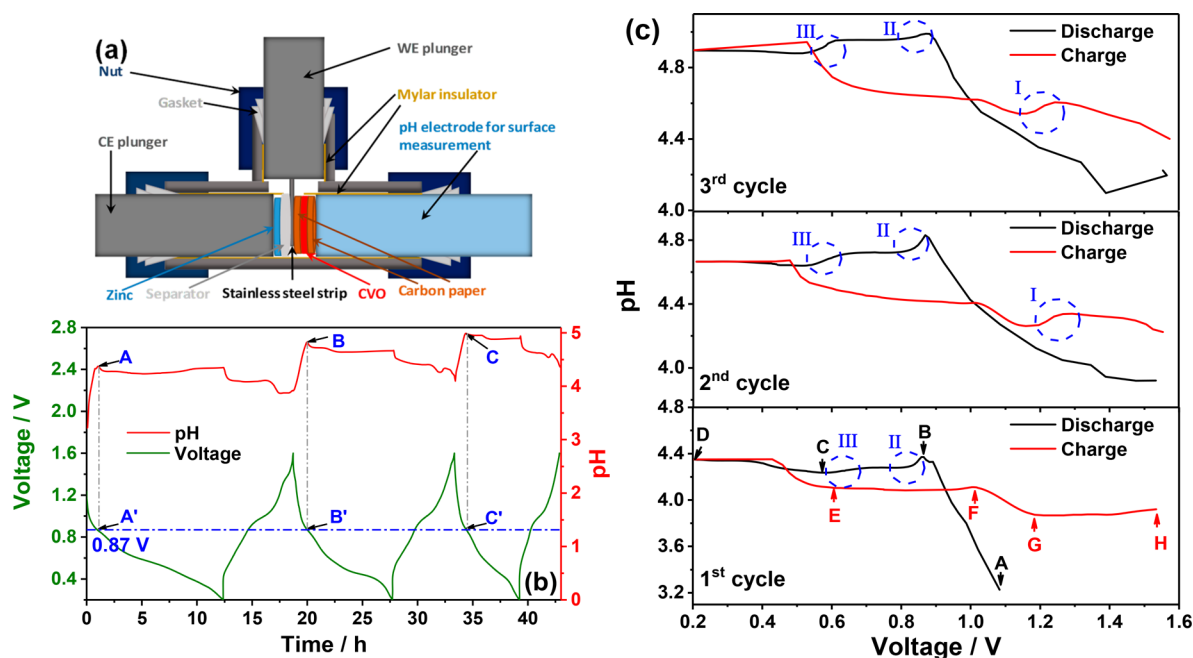
Figure 3. (a) Scheme of the cell configuration for operando pH measurements. (b) Evolution of the cell voltage and the electrolyte pH value upon the initial three charge−discharge cycles at 50 mA g^{-1}. (c) Evolution of pH versus voltage during the initial three charge−discharge cycles. 3 m Zn(OTF)$_2$ aqueous electrolyte.

The electrochemical performance of as-prepared CVO/rGO as cathode material for AZMBs was evaluated in coin cells employing a zinc foil as the negative electrode and a 3 m Zn(OTF)$_2$ aqueous solution as the electrolyte. Figure 1c displays the cyclic voltammetry (CV) curves measured at a scan rate of 0.05 mV s^{-1}. The first cycle is different from those following, indicating an activation process occurs. Also, the presence of multiple peaks indicates a multistep electrochemical process (Supplementary Note 1). The charge−discharge profiles recorded during the initial three cycles (at 50 mA g^{-1}) are displayed in Figure 1d. In agreement with the CV results, there is an evident increase in the delivered capacity after the first cycle showing a charge capacity higher than the discharge capacity. However, a highly reversible behavior is observed in the following two cycles in which a specific capacity of 357 mAh g^{-1} is delivered. The different electrochemical response in the first cycle is most likely the result of the deintercalation of calcium ions from CVO, occurring upon the first charge above 1.2 V. This is strongly corroborated via XPS measurements, which demonstrate a significant decrease of the relative signal intensity of Ca 2p against V 2p after the first cycle (Figure S5).[24] The specific capacity and charge−discharge profiles at various current densities, measured via GCPL, are displayed in Figures 1e and S6a, respectively. At specific currents of 500 and 1000 mA g^{-1}, specific capacities of 267 and 215 mAh g^{-1} are delivered, respectively. After 200 cycles at 500 mA g^{-1} (Figure S7) and 2000 cycles at 2000 mA g^{-1} (Figures 1f and S6b), the cell retains 92% and 87% of the initial capacities, respectively, thus showing a good cyclability. The CVO/rGO composite, exhibiting satisfactory properties as cathode material, is suited to serve as a model material for the investigation of the intercalation mechanism.

Following the exploration route in earlier works, we start with the *ex situ* XRD characterization of the CVO/rGO electrode in Zn(OTF)$_2$ aqueous electrolyte, as shown in Figure

2a. Upon charge and discharge, the XRD patterns exhibit a reversible shift of the CVO's (001) reflection. Moreover, additional peaks appear/disappear during cycling, suggesting the formation of additional phases. The reversible shift of the CVO's (001) plane indicates the typical solid solution mechanism originates from cation intercalations. Because of the opposite charge, the intercalated cations reduce the repulsion of the V−O layers and lead to a decrease of the interlayer spacing from 10.6 to 9.8 Å during the discharge process. An expansion back to 10.6 Å is, in fact, observed during the subsequent charge process. At high voltage, the additional reflection appearing at 12.3° can be indexed to the (001) plane of Zn$_3$(OH)$_2$V$_2$O$_7$·2H$_2$O (12.29°, PDF 50-0570), which has also been investigated as an intercalation cathode material.[37,38] Upon discharge, the Zn$_3$(OH)$_2$V$_2$O$_7$·2H$_2$O reflection disappears because of the dissolution of the low oxidation state vanadium species in the aqueous electrolyte.[24] At low voltage (0.2−0.5 V in discharge, and 0.2−0.7 V in charge), a series of reflections at 6.4°, 12.9°, and 19.5° (highlighted in blue) can be indexed to Zn$_{12}$(CF$_3$SO$_3$)$_9$(OH)$_{15}$·xH$_2$O, according to previous works.[30,39] The *ex situ* SEM (Figure S8) and *ex situ* XPS (Figure S5) further prove the reversible formation of this BZS which can be obtained via the titration of 3 m Zn(OTF)$_2$ aqueous solution with NaOH aqueous solution (Figure S9). Therefore, the formed BZS is indeed a good indicator for H$^+$ intercalation occurring in the low-voltage region (0.2−0.5 V) upon discharge. However, the involvement of H$^+$ in the higher-voltage region as well as of Zn^{2+} ions along the entire discharge and charge processes are still unclear. Despite the presence of Zn$_3$(OH)$_2$V$_2$O$_7$·2H$_2$O taking up a minor portion of the capacity, the energy storage mechanism of CVO is mainly based on solid solution processes. Although a variation of the diffusion coefficient upon charge/discharge is observed (Figure S10), this cannot be used to distinguish the shuttling cation (Zn^{2+} and H$^+$), as discussed in the Supporting Information.

To further clarify the role of H^+ and Zn^{2+} intercalation in CVO, three-electrode Swagelok-type T cells employing either 0.01 M H_2SO_4 aqueous solution or 1 M $Zn(OTF)_2$ in ACN as the electrolyte were assembled. For the H^+ intercalation investigation, free-standing activated carbon (AC) electrodes and leakless Ag/AgCl electrodes were used as the counter and reference electrodes, respectively, to exclude the influence of Zn^{2+}. Because of the limited electrochemical stability window of the 0.01 M H_2SO_4 aqueous solution, severe irreversible hydrogen evolution is observed in the discharge curve shown in Figure 2b. Nonetheless, even within the narrow potential window (−0.3−0.73 V vs Ag/AgCl, corresponding to 0.57−1.6 V vs Zn^{2+}/Zn), the CVO/rGO electrode uptakes H^+ up to 45 mAh g^{-1} as observed in the following charge. In the XRD patterns of the CVO/rGO electrode discharged to −0.3 V vs Ag/AgCl and charged to 0.73 V vs Ag/AgCl (Figure 2c), only peaks belonging to CVO can be observed. The (001) reflection exhibits a typical lattice breath, which proves the solid solution process occurs for CVO in 0.01 M H_2SO_4. For the investigation of Zn^{2+} intercalation in CVO, cells employing Zn foils as both the counter and the reference electrodes and 1 M $Zn(OTF)_2$ in ACN as the electrolyte were used. Although with a lower specific capacity (22 mAh g^{-1}) and a stronger shift of the (001) peak (Figure 2d,e and Supplementary Note 2), the CVO/rGO electrode clearly shows Zn^{2+} storage ability. From the results mentioned above, H^+ and Zn^{2+} can be independently intercalated into CVO through solid solution processes. However, the structural and electrochemical behaviors of each ion cannot be directly transferred to the Zn/CVO cell using 3 m $Zn(OTF)_2$ aqueous solution because of the inherent differences between the employed electrolytes (Supplementary Note 3).

Overall, a lack of effective characterization tools to discriminate the H^+ and Zn^{2+} intercalation processes appears in the Zn/CVO cell using 3 m $Zn(OTF)_2$ aqueous solution. In fact, the intercalation of both H^+ and Zn^{2+} occurs via solid solution processes, which eliminate the support of XRD, as well as high-resolution transmission electron microscopy (both supplying interlayer distances according to their operation mechanisms). On the other hand, the formation of the BZSs containing Zn species but not related to Zn^{2+} intercalation in CVO eliminates all elemental analysis techniques, e.g., XPS, EDS, and ICP-OES.

However, it is important to state that the intercalated H^+ must originate from the 3 m $Zn(OTF)_2$ aqueous electrolyte. This means that an increase of the electrolyte's pH occurs when H^+ is intercalated in CVO, but not upon Zn^{2+} intercalation. Therefore, monitoring the electrolyte's pH appears to be an appropriate, indirect tool to discriminate the H^+ and Zn^{2+} intercalation processes.

Therefore, a cell for *operando* pH determination has been designed, and its scheme is shown in Figure 3a. A stainless steel strip and a porous carbon paper (the left one) are used as a current collector for the working electrode. This additional carbon paper disc can increase the contact of the CVO electrode with the stainless steel strip because the size of the strip and the electronic conductivity of CVO are limited. CVO/rGO slurry cast on another porous carbon paper disc (the right one) is applied as a working electrode with the active material side facing the current collector. The back of the electrode, the porous carbon paper substrate, is in direct contact with a pH electrode that has a flat membrane and therefore can measure the pH value of the electrolyte on the carbon paper surface (Figure S11). The use of this configuration guarantees a high sensitivity of the pH measurement, because it detects in close contact of the active material.[40] Moreover, the limited amount of electrolyte (only 100 μL) used in this cell guarantees a significant variation of pH, which is not achievable in the beaker cell's configuration.[41]

The cell was subjected to a GCPL test at 50 mA g^{-1} while the pH value was recorded with a pH meter every 5 min. Figure 3b displays the typical evolution of the cell voltage and electrolyte pH during the initial three cycles. The cycling performance of the CVO electrode in this *operando* cell is inferior compared to those obtained in the coin cell tests. Lower efficiency and reversibility are detected, but they are associated with the imperfect configuration of the *operando* cell (Supplementary Note 4). The limited reversibility of CVO in the *operando* cell and the hydrogen evolution on Zn metal negative electrodes[6] can explain the drift of the pH value, which does not recover to its initial value after each cycle. However, the correlation of the pH variation with the cell voltage upon cycling is very evident, demonstrating that the pH variation is tightly associated with the electrochemical reaction of the CVO.

At the beginning of the discharge process, a sharp increase of the pH value is observed (Figure 3b). Despite the pH drift affecting the absolute value, the same occurs in the following discharges and always ends at around 0.87 V, once more implying a strong correlation between the pH and voltage. To have a better overview of the relation between voltage and pH, Figure 3c illustrates the pH versus voltage trend upon each cycle. In the first discharge, two regions (A−B and C−D) can be identified by increasing pH values, while one region (B−C) shows a rather stable pH. Increasing pH values can be the result of the intercalation of H^+ into CVO or/and hydrogen evolution, oxygen reduction side reactions. In the plateau region (B−C), accounting for a significant fraction of the CVO's capacity (about 35%), the stability of the pH value excludes H^+ intercalation. Hence, Zn^{2+} intercalation is most likely taking place in this region. The noninfluence of Zn^{2+} intercalation in pH evolution can also be extended to the deintercalation of Zn^{2+} upon the charge process.

Similarly, in the first charge process, two regions (D−E and F−G) are characterized by decreasing pH value, while two other regions (E−F and G−H) evidence steady pH values. The E−F region can be associated with the deintercalation of Zn^{2+} ions (previously intercalated in the B−C region). The G−H region, i.e., above 1.2 V, is related to the deintercalation of Ca^{2+} ions from the CVO (see Figure S5 and related text in the Supporting Information). One can conclude that deintercalation of H^+ ions from CVO is the only event leading to the pH decrease in these two regions (D−E and F−G), for the following two reasons:

I. The voltage in these two regions is much lower than the onset potential of oxygen evolution reaction in 3 m $Zn(OTF)_2$ aqueous electrolyte (higher than 2.3 V vs Zn^{2+}/Zn);[42]

II. It was evidenced above that the intercalation/deintercalation of Zn^{2+} does not significantly affect the measured pH.

The pH decrease in the D−E and F−G regions (charge) well relates with the pH increase in regions A−B and C−D (discharge), taking place at the same voltage, respectively. Therefore, the occurrence of deintercalation of H^+ in D−E and
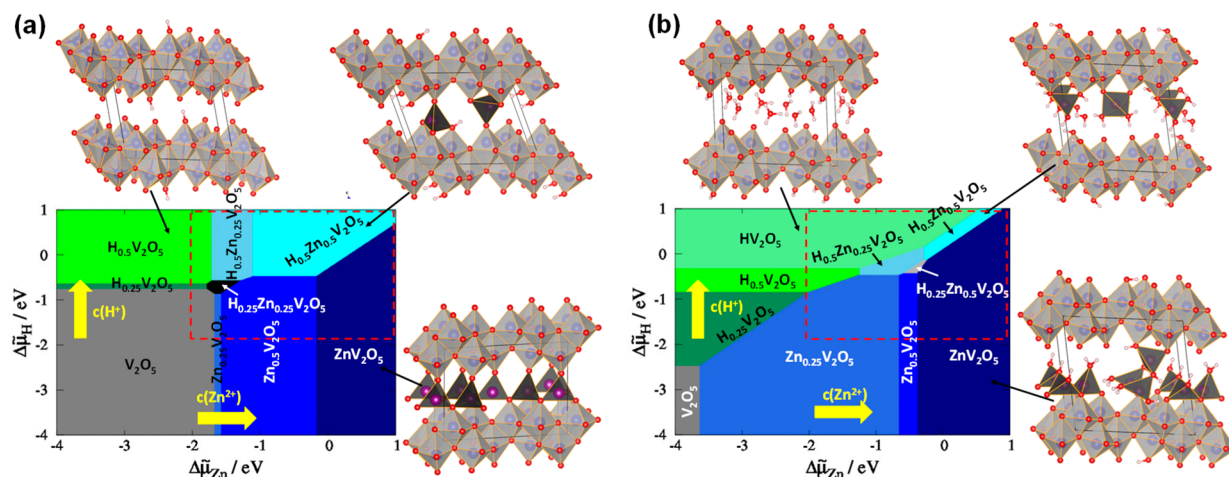
Figure 4. Calculated phase diagrams for hydrogen and Zn intercalation in (a) water-free δ-V_2O_5 and (b) δ-V_2O_5·H_2O as a function of the respective electrochemical potential. The stoichiometry of the stable phases is denoted in the corresponding area of the phase diagram. Structure images depicting hydrogen intercalation, Zn intercalation, and hydrogen−Zn cointercalation are shown as examples next to the respective regions of the phase diagram. The dashed red box is a rough estimate of the chemical potential range relevant to the experiment. The yellow arrows point in the direction of increasing Zn^{2+} and H^+ concentration (i.e., decreasing pH).

F−G regions also indicates the presence of H^+ intercalation into CVO in regions A−B and C−D.

These results demonstrate that both the H^+ and Zn^{2+} intercalations take place and contribute to the specific capacity of CVO in AZMBs. However, the contribution of Zn^{2+} intercalation/release in the regions where the pH varies, e.g., A−B, C−D, D−E, and F−G, cannot be excluded.

Upon the following (seconnd and third) cycles, the pH evolution is generally similar to that observed in the first cycle, apart from region I (blue circle in Figure 3 b), in which the pH is seen to increase upon charging. In fact, the intercalated H^+ and Zn^{2+} cations should be released back into the electrolyte during charging. However, the increasing pH value supports for H^+ intercalation. This phenomenon is also observed in the third cycle. Moreover, in regions II and III (also marked with blue circles in the discharge processes), the pH decreases rather than stabilizes or increases. These imply that the Zn^{2+} deintercalation in region I is accompanied by H^+ intercalation, while the Zn^{2+} intercalation in regions II and III is accompanied by H^+ deintercalation. Such an H^+/Zn^{2+}-exchange has seldom been reported in battery systems. DFT calculations were performed to gain insights into the mechanism responsible for the H^+/Zn^{2+} intercalation chemistry observed above. For this purpose, a large number of model structures with different intercalation chemistry were optimized by applying the VASP code (see the Supporting Information for details).[43,44]

As the Ca^{2+} is released into the electrolyte during the first charge (Figure S5), δ-V_2O_5, i.e., the V−O skeleton of CVO, was used. In a first approach, structural water was neglected, meaning that only the intercalation of H^+ and Zn^{2+} ions was considered. Interestingly, for this scenario, Zn prefers to be tetrahedrally coordinated by oxygen atoms from the V_2O_5 layers, while hydrogen coordinates on the V−O layers trying to maximize its distance to the next Zn atom (Figure S12). This is exemplarily shown for three different compounds (see Figure 4a). Moreover, it is observed that the structural integrity of the layers is lost when more than 0.5 H^+/fu (formula unit of V_2O_5) are inserted, while the intercalation of one Zn^{2+}/fu is still possible. The concept of the computational hydrogen

electrode (CHE) was adapted to access the respective stability of the intercalation compounds in an electrochemical environment.[45,46] With this approach, it is possible to access the phase stability with respect to the electrochemical potential, however, without having to explicitly calculate solvated ions (see the Supporting Information for a detailed discussion). Hence, this allows constructing a phase diagram as a function of the zinc and hydrogen electrochemical potentials ($\Delta\tilde{\mu}_{Zn}$ and $\Delta\tilde{\mu}_{H}$, respectively), which depend on the temperature, pressure, and corresponding ion concentrations (e.g., Zn^{2+} and H^+). The phase diagram obtained with this approach is depicted in Figure 4a. A closer look at the phase boundaries of the respective phases reveals that, depending on the electrochemical potential, different intercalation compounds are stable. In this graph, an increasing H^+ concentration (decreasing pH) and otherwise unchanged parameters correspond to displacement along the y-axis. Hence, many regions are seen in the phase diagram for which an increasing pH value will indeed result in H^+ moving out from the structure, while Zn^{2+} will move in. This obviously corresponds to the experimentally observed exchange mechanism and dual-carrier intercalation chemistry.

In a subsequent step, the structural water has been introduced in the DFT model, thus allowing for a more realistic modeling of the intercalation process. The investigated host structure is δ-V_2O_5·H_2O. Indeed, when water is present in the structure, H^+ ions either form H_3O^+ ions with the structural water or coordinate on the V−O layers as in the water-free scenario (see Figures 4b and S13). However, now the structure can accept more than 1 H^+/fu, which is clearly a consequence of the structural water. Zn^{2+}, on the other hand, mostly occurs in 4-fold or 5-fold environments. The oxygen from the V−O layers and structural water are involved in the coordination, as depicted in Figure 4b. Interestingly, at high Zn content, it is observed that even dissociation of structural water is possible, resulting in the formation of O−H groups in the coordination polyhedra of the Zn^{2+} (see Figure 4b). Revisiting the phase diagram, one can observe that the phase fractions and the potential ranges in which they occur have changed; however, the overall trend remains the same. Still, several

phase boundaries are observed where the exchange of H^+ and Zn^{2+} may occur, which can also explain the anomalous occurrence of a Zn^{2+} intercalation step between two H^+ intercalation steps. As a side note, it must be mentioned that different orders and further Zn^{2+} to H^+ ratios may produce additional phases, which are stable in certain regions of the phase diagram. Similarly, changing the water content will also affect the details of the phase diagram. However, phase boundaries that result in H^+/Zn^{2+} exchange will always be present, and therefore our findings strongly corroborate the proposed exchange mechanism.

In summary, with selected electrolytes and designed cell configurations, it was proved that both Zn^{2+} and H^+ can independently intercalate into CVO. *Operando* pH measurements were employed witnessing the intercalation of both H^+ and Zn^{2+} into CVO from Zn^{2+}-based aqueous electrolyte and further revealing an unusual H^+/Zn^{2+}-exchange mechanism upon charge and discharge. DFT calculations revealed that the observed H^+/Zn^{2+} intercalation chemistry is a consequence of the variation of the electrochemical potential of Zn^{2+} and H^+ during the electrochemical intercalation/release.

■ ASSOCIATED CONTENT

Ⓢ Supporting Information

The Supporting Information is available free of charge at https://pubs.acs.org/doi/10.1021/acsenergylett.0c01767.

> Experimental details; computational details; Supplementary Notes 1−4; evolution of temperature and power during microwave reactions; EDS mapping/TGA of CVO/rGO; Raman spectra of GO and CVO/rGO; XPS spectra of CVO/rGO electrodes at different charge states; cycling ability of the CVO/rGO at 500 mA g^{-1}; selected charge−discharge profiles of the CVO/rGO; SEM images of the CVO/rGO electrodes at different charge states; titration curve of 3 m $Zn(OTF)_2$/water with NaOH solution; GITT and slow scan rate CVs of the CVO/rGO; reliability test of the flat membrane pH electrode; energetically most stable structures of δ-V_2O_5/δ-$V_2O_5 \cdot H_2O$ with different H^+ and Zn^{2+} content (PDF)

■ AUTHOR INFORMATION

Corresponding Authors

Giuseppe Antonio Elia − *Helmholtz Institute Ulm (HIU), D-89081 Ulm, Germany; Karlsruhe Institute of Technology (KIT), D-76021 Karlsruhe, Germany;* ⓘ orcid.org/0000-0001-6790-1143; Email: giuseppe.elia@kit.edu

Stefano Passerini − *Helmholtz Institute Ulm (HIU), D-89081 Ulm, Germany; Karlsruhe Institute of Technology (KIT), D-76021 Karlsruhe, Germany;* ⓘ orcid.org/0000-0002-6606-5304; Email: stefano.passerini@kit.edu

Authors

Xu Liu − *Helmholtz Institute Ulm (HIU), D-89081 Ulm, Germany; Karlsruhe Institute of Technology (KIT), D-76021 Karlsruhe, Germany;* ⓘ orcid.org/0000-0003-0532-316X

Holger Euchner − *Helmholtz Institute Ulm (HIU), D-89081 Ulm, Germany;* ⓘ orcid.org/0000-0003-2287-6970

Maider Zarrabeitia − *Helmholtz Institute Ulm (HIU), D-89081 Ulm, Germany; Karlsruhe Institute of Technology (KIT), D-76021 Karlsruhe, Germany; Centre for Cooperative Research on Alternative Energies (CIC energiGUNE), Basque Research and Technology Alliance (BRTA), 01510 Vitoria-Gasteiz, Spain*

Xinpei Gao − *Helmholtz Institute Ulm (HIU), D-89081 Ulm, Germany; Karlsruhe Institute of Technology (KIT), D-76021 Karlsruhe, Germany*

Axel Groß − *Helmholtz Institute Ulm (HIU), D-89081 Ulm, Germany; University of Ulm, Institute of Theoretical Chemistry, D-89081 Ulm, Germany;* ⓘ orcid.org/0000-0003-4037-7331

Complete contact information is available at:
https://pubs.acs.org/10.1021/acsenergylett.0c01767

Notes

The authors declare no competing financial interest.

■ ACKNOWLEDGMENTS

■ REFERENCES

(1) Tang, B.; Shan, L.; Liang, S.; Zhou, J. Issues and Opportunities Facing Aqueous Zinc-Ion Batteries. *Energy Environ. Sci.* **2019**, *12* (11), 3288−3304.

(2) Qiu, H.; Du, X.; Zhao, J.; Wang, Y.; Ju, J.; Chen, Z.; Hu, Z.; Yan, D.; Zhou, X.; Cui, G. Zinc Anode-Compatible in-Situ Solid Electrolyte Interphase via Cation Solvation Modulation. *Nat. Commun.* **2019**, *10* (5374), 1−12.

(3) Song, M.; Tan, H.; Chao, D.; Fan, H. J. Recent Advances in Zn-Ion Batteries. *Adv. Funct. Mater.* **2018**, *28* (41), 1802564.

(4) Fang, G.; Zhou, J.; Pan, A.; Liang, S. Recent Advances in Aqueous Zinc-Ion Batteries. *ACS Energy Lett.* **2018**, *3* (10), 2480−2501.

(5) Zhang, N.; Jia, M.; Dong, Y.; Wang, Y.; Xu, J.; Liu, Y.; Jiao, L.; Cheng, F. Hydrated Layered Vanadium Oxide as a Highly Reversible Cathode for Rechargeable Aqueous Zinc Batteries. *Adv. Funct. Mater.* **2019**, *29* (10), 1807331.

(6) Zhao, Z.; Zhao, J.; Hu, Z.; Li, J.; Li, J.; Zhang, Y.; Wang, C.; Cui, G. Long-Life and Deeply Rechargeable Aqueous Zn Anodes Enabled by a Multifunctional Brightener-Inspired Interphase. *Energy Environ. Sci.* **2019**, *12* (6), 1938−1949.

(7) Liu, X.; Zhang, H.; Geiger, D.; Han, J.; Varzi, A.; Kaiser, U.; Moretti, A.; Passerini, S. Calcium Vanadate Sub-Microfibers as Highly Reversible Host Cathode Material for Aqueous Zinc-Ion Batteries. *Chem. Commun.* **2019**, *55* (16), 2265−2268.

(8) Kundu, D.; Adams, B. D.; Duffort, V.; Vajargah, S. H.; Nazar, L. F. A High-Capacity and Long-Life Aqueous Rechargeable Zinc Battery Using a Metal Oxide Intercalation Cathode. *Nat. Energy* **2016**, *1* (10), 1−8.

(9) Chen, L.; An, Q.; Mai, L. Recent Advances and Prospects of Cathode Materials for Rechargeable Aqueous Zinc-Ion Batteries. *Adv. Mater. Interfaces* **2019**, *6* (17), 1900387.

(10) Konarov, A.; Voronina, N.; Jo, J. H.; Bakenov, Z.; Sun, Y. K.; Myung, S. T. Present and Future Perspective on Electrode Materials for Rechargeable Zinc-Ion Batteries. *ACS Energy Lett.* **2018**, *3* (10), 2620−2640.

(11) Zhu, K.; Wu, T.; Huang, K. NaCa0.6V6O16·3H2O as an Ultra-Stable Cathode for Zn-Ion Batteries: The Roles of Pre-Inserted Dual-Cations and Structural Water in V3O8 Layer. *Adv. Energy Mater.* **2019**, *9* (38), 1901968.

(12) Liao, M.; Wang, J.; Ye, L.; Sun, H.; Wen, Y.; Wang, C.; Sun, X.; Wang, B.; Peng, H. A Deep-Cycle Aqueous Zinc-Ion Battery Containing an Oxygen-Deficient Vanadium Oxide Cathode. *Angew. Chem., Int. Ed.* **2020**, *59*, 2273−2278.

(13) Liu, F.; Chen, Z.; Fang, G.; Wang, Z.; Cai, Y.; Tang, B.; Zhou, J.; Liang, S. V2O5 Nanospheres with Mixed Vanadium Valences as High Electrochemically Active Aqueous Zinc-Ion Battery Cathode. *Nano-Micro Lett.* **2019**, *11* (1), 1−11.

(14) Chen, L.; Yang, Z.; Huang, Y. Monoclinic VO2(D) Hollow Nanospheres with Super-Long Cycle Life for Aqueous Zinc Ion Batteries. *Nanoscale* **2019**, *11* (27), 13032−13039.

(15) Pan, Z.; Yang, J.; Yang, J.; Zhang, Q.; Zhang, H.; Li, X.; Kou, Z.; Zhang, Y.; Chen, H.; Yan, C.; et al. Stitching of Zn3(OH)2V2O7·2H2O 2D Nanosheets by 1D Carbon Nanotubes Boosts Ultrahigh Rate for Wearable Quasi-Solid-State Zinc-Ion Batteries. *ACS Nano* **2020**, *14*, 842−853.

(16) Liu, Y.; Li, Q.; Ma, K.; Yang, G.; Wang, C. Graphene Oxide Wrapped Cuv2o6 Nanobelts as High-Capacity and Long-Life Cathode Materials of Aqueous Zinc-Ion Batteries. *ACS Nano* **2019**, *13* (10), 12081−12089.

(17) Wan, F.; Niu, Z. Design Strategies for Vanadium-Based Aqueous Zinc-Ion Batteries. *Angew. Chem., Int. Ed.* **2019**, *58* (46), 16358−16367.

(18) Pang, Q.; Sun, C.; Yu, Y.; Zhao, K.; Zhang, Z.; Voyles, P. M.; Chen, G.; Wei, Y.; Wang, X. H2V3O8 Nanowire/Graphene Electrodes for Aqueous Rechargeable Zinc Ion Batteries with High Rate Capability and Large Capacity. *Adv. Energy Mater.* **2018**, *8* (19), 1800144.

(19) Sambandam, B.; Soundharrajan, V.; Kim, S.; Alfaruqi, M. H.; Jo, J.; Kim, S.; Mathew, V.; Sun, Y. K.; Kim, J. Aqueous Rechargeable Zn-Ion Batteries: An Imperishable and High-Energy Zn2V2O7 Nanowire Cathode through Intercalation Regulation. *J. Mater. Chem. A* **2018**, *6* (9), 3850−3856.

(20) Kundu, D.; Hosseini Vajargah, S.; Wan, L.; Adams, B.; Prendergast, D.; Nazar, L. F. Aqueous: Vs. Nonaqueous Zn-Ion Batteries: Consequences of the Desolvation Penalty at the Interface. *Energy Environ. Sci.* **2018**, *11* (4), 881−892.

(21) Liu, W.; Dong, L.; Jiang, B.; Huang, Y.; Wang, X.; Xu, C.; Kang, Z.; Mou, J.; Kang, F. Layered Vanadium Oxides with Proton and Zinc Ion Insertion for Zinc Ion Batteries. *Electrochim. Acta* **2019**, *320*, 134565.

(22) He, P.; Quan, Y.; Xu, X.; Yan, M.; Yang, W.; An, Q.; He, L.; Mai, L. High-Performance Aqueous Zinc-Ion Battery Based on Layered H2V3O8 Nanowire Cathode. *Small* **2017**, *13* (47), 1702551.

(23) He, P.; Zhang, G.; Liao, X.; Yan, M.; Xu, X.; An, Q.; Liu, J.; Mai, L. Sodium Ion Stabilized Vanadium Oxide Nanowire Cathode for High-Performance Zinc-Ion Batteries. *Adv. Energy Mater.* **2018**, *8* (10), 1702463.

(24) Zhang, L.; Rodríguez-Pérez, I. A.; Jiang, H.; Zhang, C.; Leonard, D. P.; Guo, Q.; Wang, W.; Han, S.; Wang, L.; Ji, X. ZnCl2 "Water-in-Salt" Electrolyte Transforms the Performance of Vanadium Oxide as a Zn Battery Cathode. *Adv. Funct. Mater.* **2019**, *29* (30), 1902653.

(25) Alfaruqi, M. H.; Mathew, V.; Song, J.; Kim, S.; Islam, S.; Pham, D. T.; Jo, J.; Kim, S.; Baboo, J. P.; Xiu, Z.; et al. Electrochemical Zinc Intercalation in Lithium Vanadium Oxide: A High-Capacity Zinc-Ion Battery Cathode. *Chem. Mater.* **2017**, *29* (4), 1684−1694.

(26) Yan, M.; He, P.; Chen, Y.; Wang, S.; Wei, Q.; Zhao, K.; Xu, X.; An, Q.; Shuang, Y.; Shao, Y.; et al. Water-Lubricated Intercalation in V2O5·nH2O for High-Capacity and High-Rate Aqueous Rechargeable Zinc Batteries. *Adv. Mater.* **2018**, *30* (1), 1703725.

(27) Soundharrajan, V.; Sambandam, B.; Kim, S.; Alfaruqi, M. H.; Putro, D. Y.; Jo, J.; Kim, S.; Mathew, V.; Sun, Y. K.; Kim, J. Na2V6O16·3H2O Barnesite Nanorod: An Open Door to Display a Stable and High Energy for Aqueous Rechargeable Zn-Ion Batteries as Cathodes. *Nano Lett.* **2018**, *18* (4), 2402−2410.

(28) Ming, F.; Liang, H.; Lei, Y.; Kandambeth, S.; Eddaoudi, M.; Alshareef, H. N. Layered Mg XV2O5· NH2O as Cathode Material for High-Performance Aqueous Zinc Ion Batteries. *ACS Energy Lett.* **2018**, *3* (10), 2602−2609.

(29) Li, Z.; Ganapathy, S.; Xu, Y.; Zhou, Z.; Sarilar, M.; Wagemaker, M. Mechanistic Insight into the Electrochemical Performance of Zn/VO2 Batteries with an Aqueous ZnSO4 Electrolyte. *Adv. Energy Mater.* **2019**, *9* (22), 1900237.

(30) Yang, G.; Li, Q.; Ma, K.; Hong, C.; Wang, C. The Degradation Mechanism of Vanadium Oxide-Based Aqueous Zinc-Ion Batteries. *J. Mater. Chem. A* **2020**, *8*, 8084−8095.

(31) Wan, F.; Zhang, L.; Dai, X.; Wang, X.; Niu, Z.; Chen, J. Aqueous Rechargeable Zinc/Sodium Vanadate Batteries with Enhanced Performance from Simultaneous Insertion of Dual Carriers. *Nat. Commun.* **2018**, *9* (1656), 1−11.

(32) Wei, T.; Li, Q.; Yang, G.; Wang, C. Pseudo-Zn - Air and Zn-Ion Intercalation Dual Mechanisms to Realize Highk-Areal Capacitance and Long-Life Energy Storage in Aqueous Zn Battery. *Adv. Energy Mater.* **2019**, *9*, 1901480.

(33) Park, M. J.; Yaghoobnejad Asl, H.; Manthiram, A. Multivalent-Ion versus Proton Insertion into Battery Electrodes. *ACS Energy Lett.* **2020**, *5*, 2367−2375.

(34) Canepa, P.; Sai Gautam, G.; Hannah, D. C.; Malik, R.; Liu, M.; Gallagher, K. G.; Persson, K. A.; Ceder, G. Odyssey of Multivalent Cathode Materials: Open Questions and Future Challenges. *Chem. Rev.* **2017**, *117* (5), 4287−4341.

(35) Xia, C.; Guo, J.; Li, P.; Zhang, X.; Alshareef, H. N. Highly Stable Aqueous Zinc-Ion Storage Using a Layered Calcium Vanadium Oxide Bronze Cathode. *Angew. Chem.* **2018**, *130* (15), 4007−4012.

(36) Zhu, K.; Wu, T.; Huang, K. A High Capacity Bilayer Cathode for Aqueous Zn-Ion Batteries. *ACS Nano* **2019**, *13* (12), 14447−14458.

(37) Xia, C.; Guo, J.; Lei, Y.; Liang, H.; Zhao, C.; Alshareef, H. N. Rechargeable Aqueous Zinc-Ion Battery Based on Porous Framework Zinc Pyrovanadate Intercalation Cathode. *Adv. Mater.* **2018**, *30* (5), 1705580.

(38) Guo, J.; Ming, J.; Lei, Y.; Zhang, W.; Xia, C.; Cui, Y.; Alshareef, H. N. Artificial Solid Electrolyte Interphase for Suppressing Surface Reactions and Cathode Dissolution in Aqueous Zinc Ion Batteries. *ACS Energy Lett.* **2019**, *4* (12), 2776−2781.

(39) Li, Q.; Liu, Y.; Ma, K.; Yang, G.; Wang, C. In Situ Ag Nanoparticles Reinforced Pseudo-Zn - Air Reaction Boosting Ag 2 V 4 O 11 as High-Performance Cathode Material for Aqueous Zinc-Ion Batteries. *Small Methods* **2019**, *3*, 1900637.

(40) Lee, B.; Seo, R.; Lee, R.; Yoon, S.; Kim, H.; Chung, K. Y.; Cho, W.; Oh, S. H. Critical Role of PH Evolution of Electrolyte in the Reaction Mechanism for Rechargeable Zinc Batteries. *ChemSusChem* **2016**, *9*, 2948−2956.

(41) Bischoff, C. F.; Fitz, S.; Burns, J.; Bauer, M.; Gentischer, H.; Birke, K. P.; Henning, H.; Biro, D. Revealing the Local PH Value Changes of Acidic Aqueous Zinc Ion Batteries with a Manganese Dioxide Electrode during Cycling. *J. Electrochem. Soc.* **2020**, *167*, 020545.

(42) Zhang, N.; Cheng, F.; Liu, Y.; Zhao, Q.; Lei, K.; Chen, C.; Liu, X.; Chen, J. Cation-Deficient Spinel ZnMn2O4 Cathode in Zn(CF3SO3)2 Electrolyte for Rechargeable Aqueous Zn-Ion Battery. *J. Am. Chem. Soc.* **2016**, *138* (39), 12894−12901.

(43) Kresse, G.; Furthmüller, J. Efficient Iterative Schemes for Ab Initio Total-Energy Calculations Using a Plane-Wave Basis Set. *Phys. Rev. B: Condens. Matter Mater. Phys.* **1996**, *54* (16), 11169−11186.

(44) Kresse, G.; Joubert, D. From Ultrasoft Pseudopotentials to the Projector Augmented-Wave Method. *Phys. Rev. B: Condens. Matter Mater. Phys.* **1999**, *59* (3), 1758−1775.

(45) Gossenberger, F.; Roman, T.; Groß, A. Hydrogen and Halide Co-Adsorption on Pt(111) in an Electrochemical Environment: A Computational Perspective. *Electrochim. Acta* **2016**, *216*, 152−159.

(46) Nørskov, J. K.; Rossmeisl, J.; Logadottir, A.; Lindqvist, L.; Kitchin, J. R.; Bligaard, T.; Jónsson, H. Origin of the Overpotential for Oxygen Reduction at a Fuel-Cell Cathode. *J. Phys. Chem. B* **2004**, *108* (46), 17886−17892.